Supplementary Information

Awakening of high-energy phosphorescence by enhanced weak interactions for ratiometric detection of trichloromethane vapor

Bo-Lun Zhang,[b] Wen-Tao Song,[a] Jian-Jun Zhang,*[a] Jun Chen,[b] Lei Miao,[a] Wen-Jing Shi,[a] Rui-Hong Wang,[a] Mengmeng Cai,[a] Jun Ni[a] and Zongbin Zhao*[b]

a. School of Chemistry, Dalian University of Technology, Dalian 116024, China.
E-mail: zhangjj@dlut.edu.cn

b. School of Chemical Engineering, Dalian University of Technology, Dalian 116024, China.
E-mail: zbzhao@dlut.edu.cn

Contents

I. Experimental Section.

II. Supplementary Materials for Results and Discussion.

III. Supplementary References.

I. Experimental Section.

Materials and instruments

Characterization: Elemental analyses of C, H, and N were determined on a Vario EL III elemental analyzer. Powder X-ray diffraction pattern (PXRD) data were collected on a Rigaku SmartLab 9KW Xray diffractometer. Thermogravimetric analyses (TGA) were performed under nitrogen atmosphere with a heating rate of 10°C/min using a TA-Q50 thermogravimetric analyzer. The UV-vis diffuse reflection/absorption spectra were collected on a Lambda 750S spectrophotometer. Luminescence spectra were acquired at ambient temperature using a Hitachi F-7100 fluorescence spectrophotometer. Luminescence lifetime tests were conducted on a FLS1000 spectrophotometer (Edinburgh Instruments) equipped with a microsecond flash lamp (uF900) and an Oxford liquid nitrogen cryostat, respectively (Instrumental Analysis Center of DUT). The quantum yields was measured on Quantaurus-QY Plus C13534-12 (Hamamatsu Photonics). Infrared spectra (IR) were recorded on a Nicolet-IS50 spectrometer as KBr pellets in the range of 4000–650 cm^{-1}. Photoluminescence graphs were plotted using a Samsung smartphone (SM-G9910) under UV lamp irradiation.

X-ray Crystallographic Study: Intensity data of single crystal was measured on Bruker D8 Venture diffractometer with a PHOTON 100 CMOS area detector, using Mo-K radiation from an Incoatec IμS microsource with focusing mirrors. The structure was solved by direct methods using SHELXS-2014 and was refined by full-matrix least squares methods using SHELXS-2014.[1] The hydrogen atoms were included in the structural model as fixed atoms "riding" on their respective carbon atoms using the idealized sp^2-hybridized geometry and C–H bond lengths of 0.95 Å. A summary of the most important crystal and structure refinement data is given in Tables S1. Selected bond lengths and angles was given in Tables S2. CCDC 2425596 and 2435342 contains the supplementary crystallographic data for this paper. The data can be obtained free of charge via www.ccdc.cam.ac.uk/conts/retrieving.html (or from the Cambridge Crystallographic Data Centre, 12 Union Road, Cambridge CB2 1EZ, UK; fax: (+44) 1223-336-033; or e-mail: deposit@ccdc.cam.ac.uk).

Theoretical Calculations: The calculations were performed with the time-dependent density functional theory (TD-DFT) by Gaussian 16 software.[2] The initial configurations were fully optimized by ωB97XD[3] with def2-TZVP basic set for Bi and 6-31G(d,p) for the others. The hole-electron analysis was performed in Multiwfn 3.8 package[4] and visualized through VMD software.[5] The SOC constants were evaluated through ORCA package (version 5.0.2)[6] at ωB97XD/def2-TZVP level.

Sensing experiment: The BBP powder was spin-coated onto a rectangular quartz substrate, which was then vertically positioned in a 50 mL glass vial. A predetermined volume of TCM (x μL) was precisely injected into the vial using a microsyringe, followed by immediate sealing with an airtight cap. The assembly was placed on a preheated hotplate maintained at 65°C for 5 min to ensure complete TCM vaporization, then allowed to cool to ambient temperature. After 30 min of equilibration at room temperature, the sealed vial was directly transferred to the sample chamber of a fluorescence spectrophotometer for optical measurements (Fig. S25). (Note: The injected TCM volumes corresponding to 10, 50, 80, 100, and 120 ppm vapor concentrations were 5.0, 25.0, 40.0, 50.0, and 60.0 μL, respectively.)

Preparation

Synthesis of compound 1: $BiCl_3$ (1.0 mmol, 0.3153 g), 2,2'-bipyridine (1.0 mmol, 0.1562 g), PPh_4Cl (1.0 mmol, 0.3748 g), and 4.0 mL acetonitrile were added to a 25 mL closed contained of Teflon. After sealing, the vessel was placed into a high-pressure reactor and heated at 105^{o}C for 24 h. Finally, pure colorless and transparent crystals were filtered, washed with 1×3 mL acetonitrile, and dried in the air at RT (**Scheme S1a**). (~94% yield based on Bi^{3+}). Element analysis (%) calcd for $C_{34}H_{28}Cl_4N_2PBi$: C, 48.25; H, 3.33; N, 3.31. Found: C, 48.10; H, 3.26; N, 3.25. IR (cm^{-1}): 3101 (w), 3078 (w), 3054 (m), 3023 (w), 1593 (s), 1484 (m), 1470 (m), 1435 (s), 1312 (s), 1248 (m), 1218 (w), 1186 (m), 1165 (m), 1106 (s), 1069 (w), 1017 (m), 996 (m), 776 (s), 756 (s), 721 (s), 691 (s).

Synthesis of compound 2: Compound 2 was synthesized in a similar way to compound 1, except that acetonitrile was replaced with trichlormethane. (~90% yield based on Bi^{3+}). Element analysis (%) calcd for $C_{35}H_{30}Cl_7N_2O_{0.5}PBi$: C, 43.13; H, 3.10; N, 2.87. Found: C, 43.10; H, 3.07; N, 2.84. IR (cm^{-1}): 3114 (m), 3089 (s), 3024 (w), 3019 (w), 1621 (s), 1597 (m), 1565 (s), 1453 (w), 1440 (s), 1396 (m), 1311 (m), 1270 (w), 1237 (w), 1190 (m), 1110 (s), 1070 (m), 937 (m), 861 (m), 762 (s), 725 (s), 691 (s).

Preparation process of 1@PVP: First, add 1.0 mL of $BiCl_3$/DMSO (0.1 mol/L) to a beaker containing 4.0 mL of PVP/DMSO (10.0 g/L) solution. After stirring for 10 min, sequentially add 1.0 mL of PPh_4Cl/DMSO (0.1 mol/L) solution and 1.0 mL of 2,2'-bipyridine/DMSO (0.1 mol/L) solution to the beaker to obtain the precursor solution. Use a pipette to aspirate 1.5 mL precursor solution and drop it onto a 5.0 cm × 2.5 cm SiO_2 glass substrate. Then, cover the liquid film with another SiO_2 glass substrate of the same size on top, and remove excess solution using filter paper. Finally, place the composite glass substrate in an 85°C vacuum oven and heat it for 24 h.

II. Supplementary Materials for Results and Discussion.

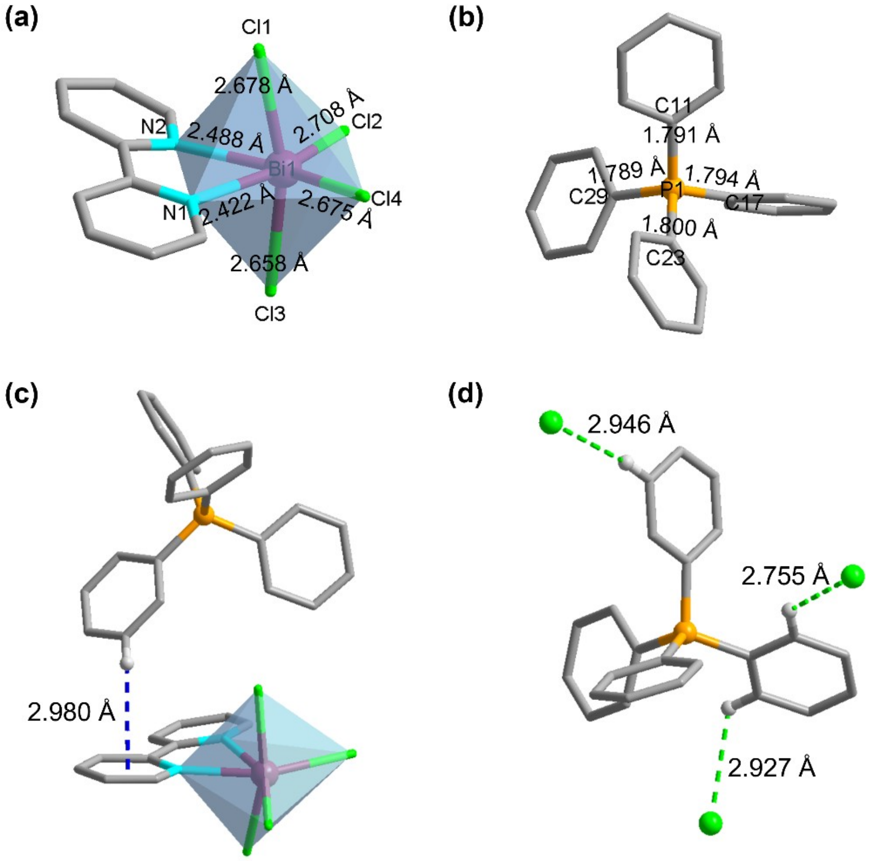

Fig S1. The structure of anion (a) and cation (b) in **1** and the bond length of the main chemical bonds. C-H···π (c) and C-H···Cl (d) interactions between cations and anions in **1**.

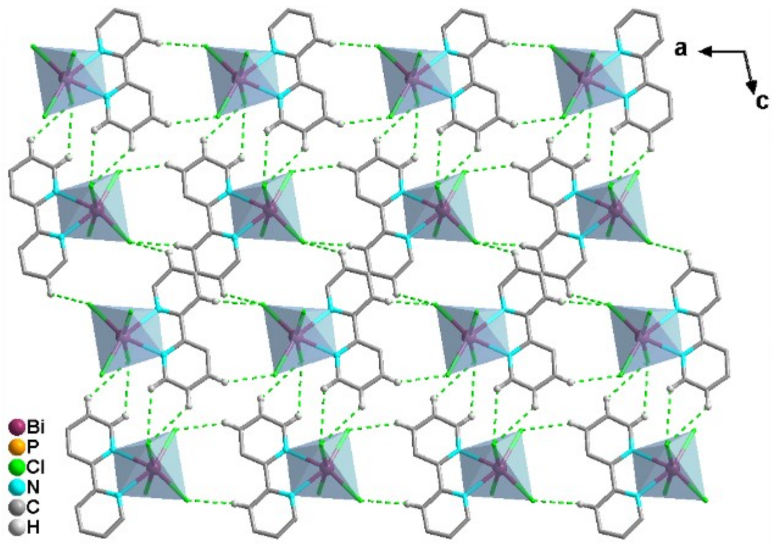

Fig S2. Adjacent anions form 2D layers through C-H···Cl (green dashed lines) interactions.

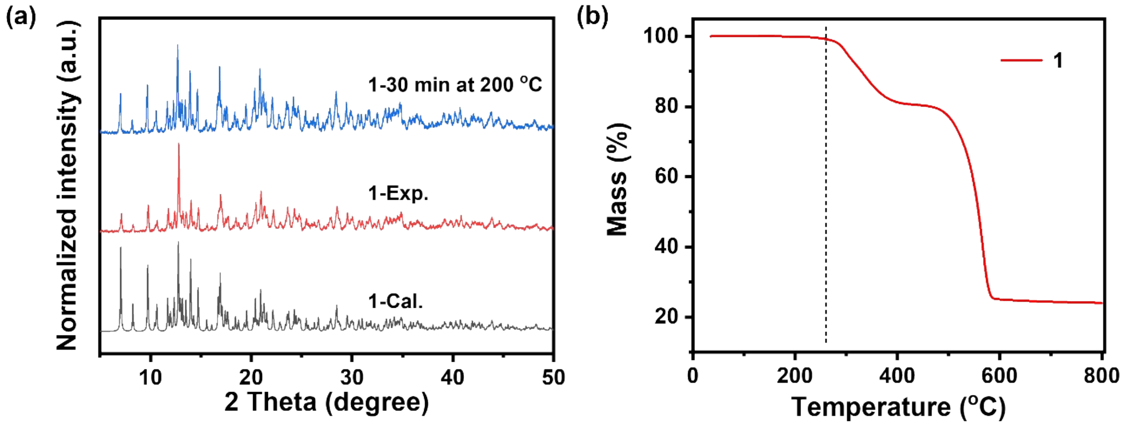

Fig S3. (a) A comparison of the calculated and experimental PXRD patterns of **1**, patterns of **1** heated at 200°C for 30 min. (b) TGA curve of **1**.

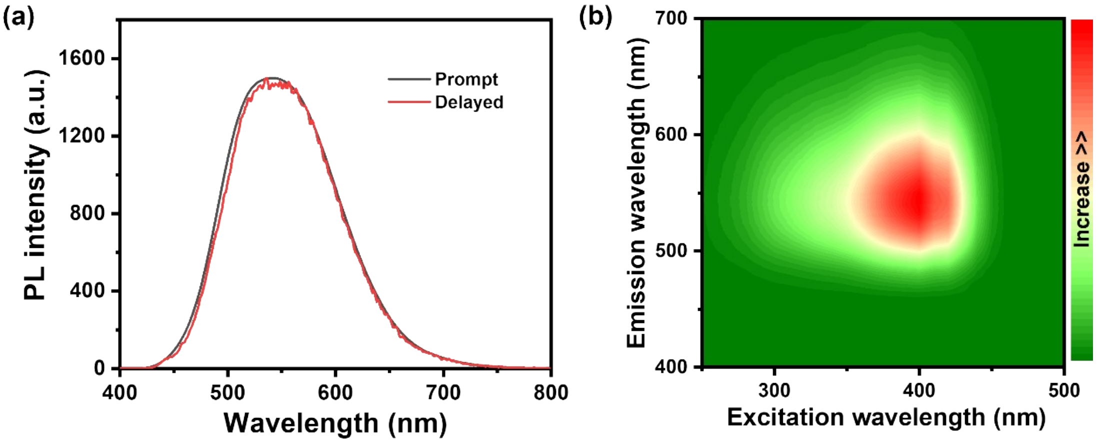

Fig S4. (a) Normalized prompt and delayed state spectra of **1** at RT. (b) Excitation wavelength-dependent delayed spectra of **1** at RT.

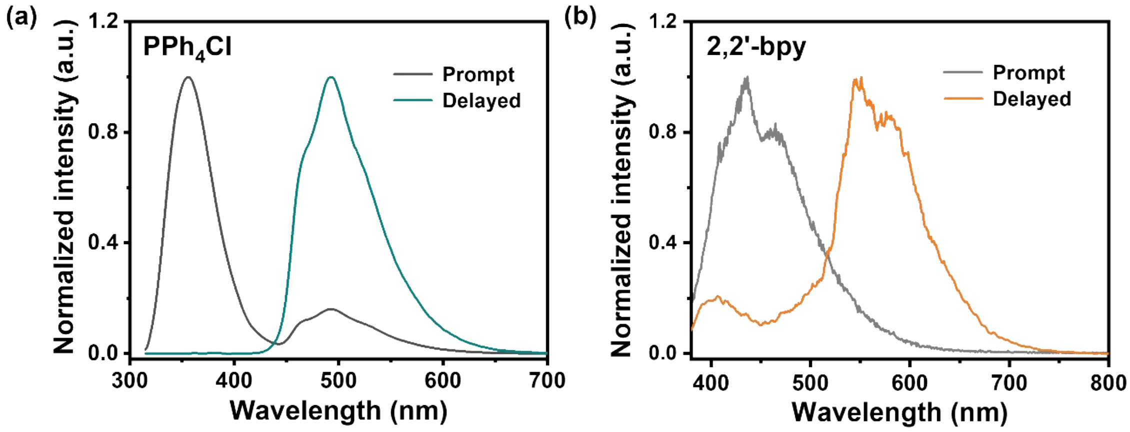

Fig S5. Normalized prompt and delayed state spectra of PPh_4Cl (a) and 2,2'-bpy (b) at RT.

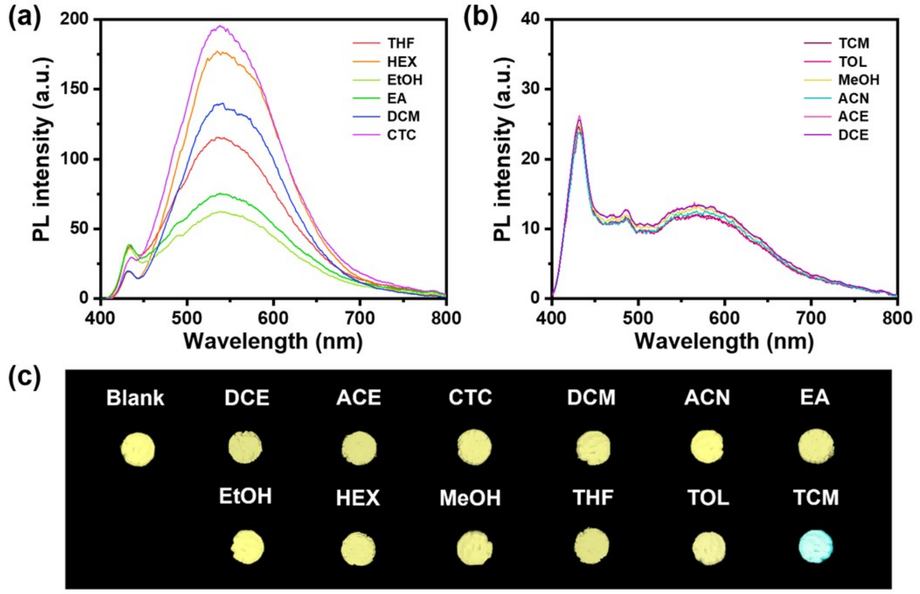

DCE: Dichloroethane **ACE:** Acetone **CTC:** Carbon tetrachloride

DCM: Dichloromethane **ACN:** Acetonitrile **EA:** Ethyl acetate

EtOH: Ethyl alcohol **HEX:** Hexane **MeOH:** Methanol

THF: Tetrahydrofuran **TOL:** Toluene **TCM:** Trichloromethane

Fig S6. (a) Delayed spectra of suspensions of **1** in THF, HEX, EtOH, EA, DCM and CTC (10 mg/mL) (λ_{ex} = 365 nm). (b) Delayed spectra of suspensions of **1** in TCM, TOL, MeOH, ACN, ACE and DCE (10 mg/mL) (λ_{ex} = 365 nm). (c) Photographs of **1** powder fumed with various VOCs vapor (120 ppm) for 30 min under a 365 nm UV lamp.

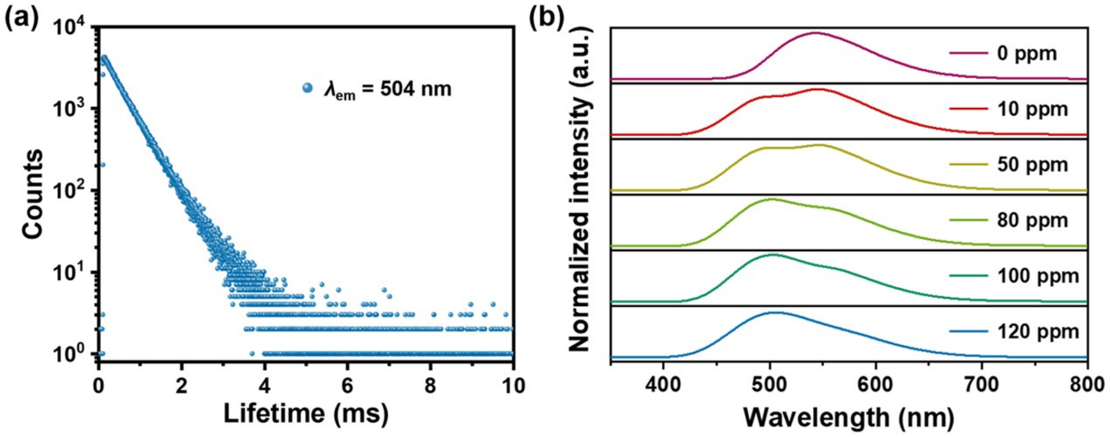

Fig S7. (a) Time-resolved PL decay curve at 504 nm of **1** after fumigation with TCM vapor (120 ppm) for 30 min. (b) Normalized delayed state spectra of **1** after fumigation with TCM vapor of different concentrations for 30 min (λ_{ex} = 365 nm).

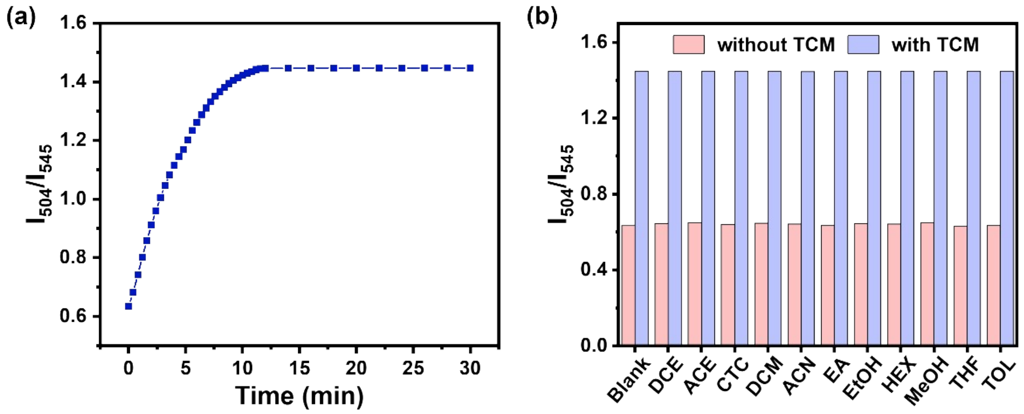

Fig S8. (a) The time response of **1** to TCM vapor at the concentration of 120 ppm. (b) Selective detection of TCM vapor by **1** in the presence of other VOCs vapor.

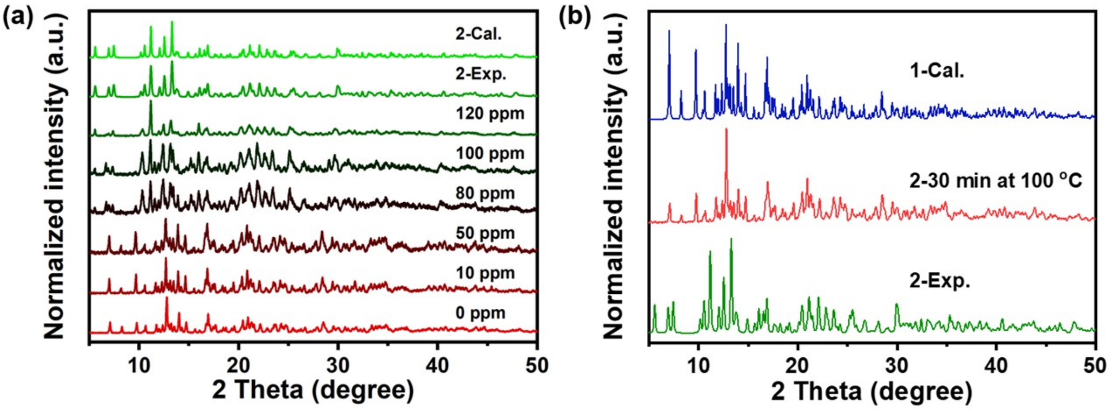

Fig S9. (a) The calculated and experimental PXRD spectra of **2**, and the comparison of PXRD spectra of **1** after fumigation with different concentrations of TCM vapor for 30 min. (b) A comparison of PXRD patterns of experimental and heated at 200°C for 30 min of **2**, calculated pattern of **1**.

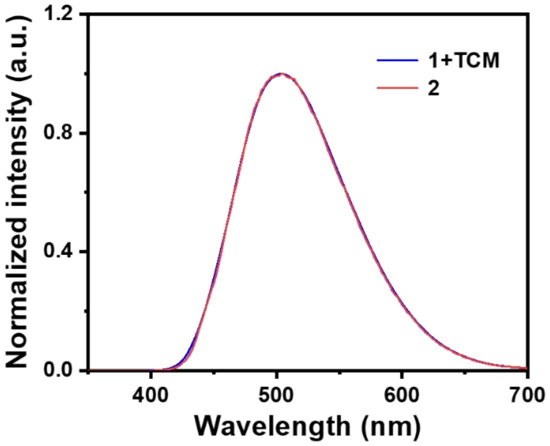

Fig S10. Normalized delayed state spectrum of **1** after fumigation with TCM vapor (120 ppm) for 30 min, as well as normalized delayed state spectrum of **2** measured at RT (λ_{ex} = 365 nm).

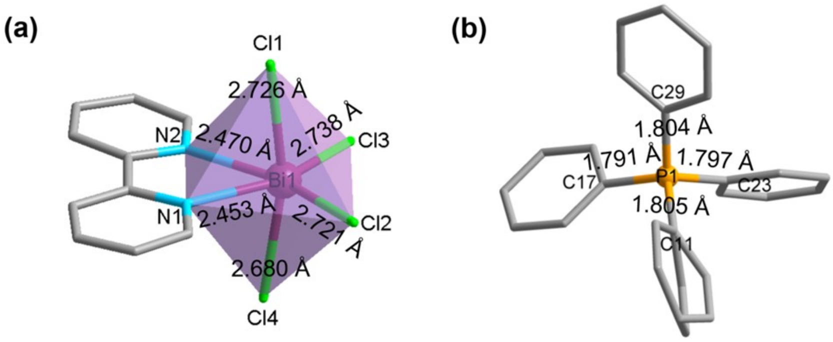

Fig S11. The structure of anion (a) and cation (b) in **2** and the bond length of the main chemical bonds.

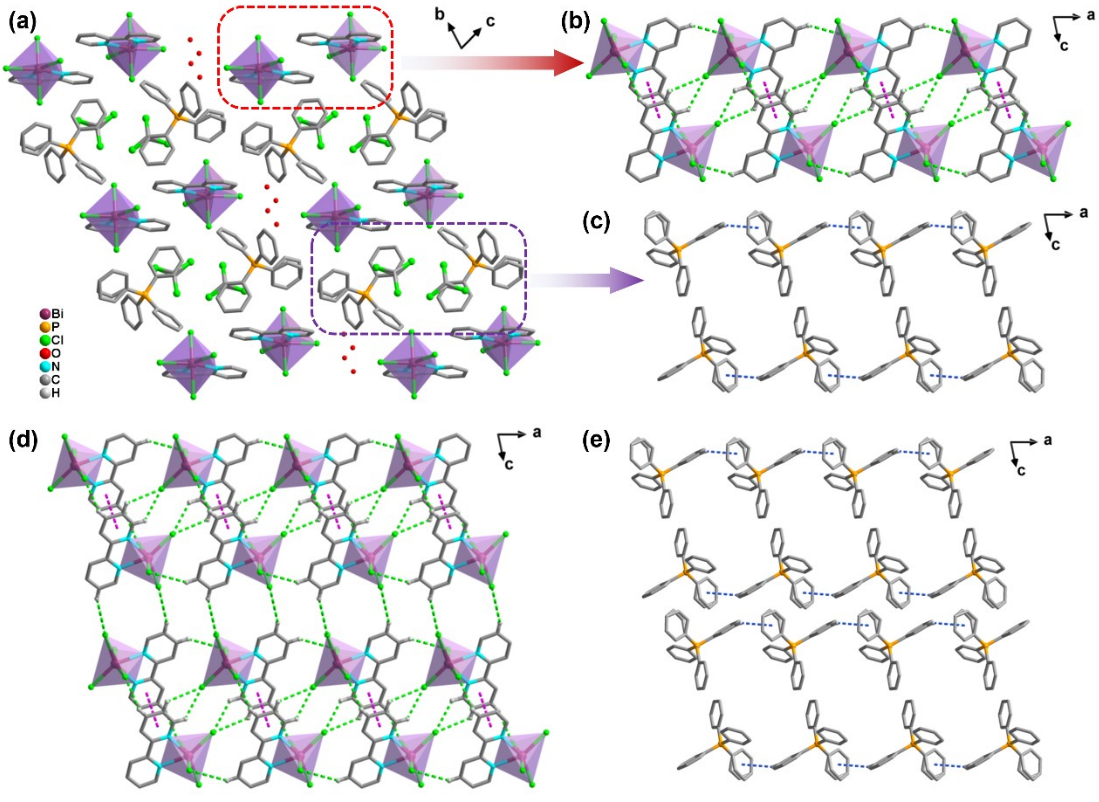

Fig S12. Single crystal structure of compound **2**. (a) Stacking structure along the a-axis direction. Adjacent anions or cations form 1D belts (b-c) and 2D layers (d-e) through C-H···Cl (green dashed lines) or C-H···π (blue dashed lines) interactions, respectively.

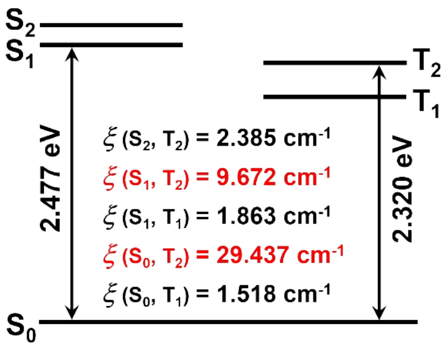

Fig S13. Calculate the singlet and triplet excited state energy levels of **1** and the corresponding spin-orbit coupling constants during the transition process.

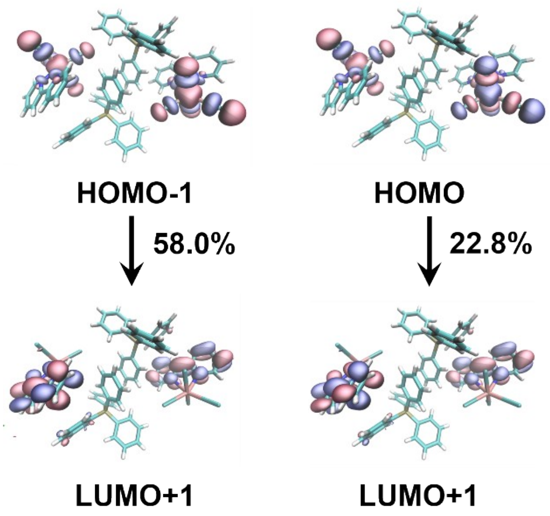

Fig S14. Frontline molecular orbital diagram of T_2 state of **1**.

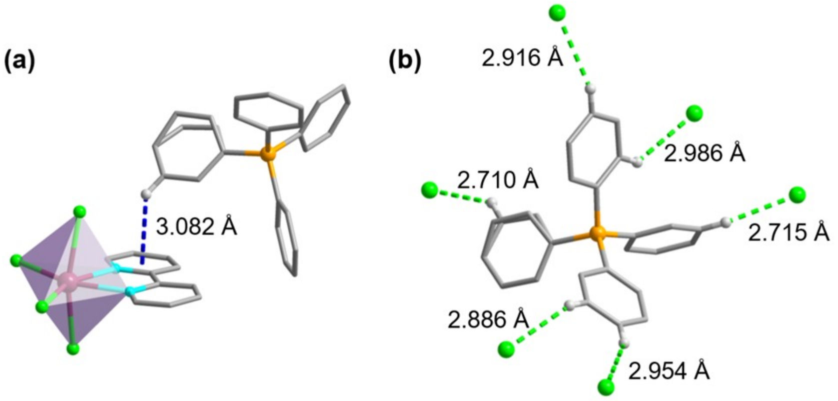

Fig S15. C-H···π (a) and C-H···Cl (b) interactions between cations and anions in **2**.

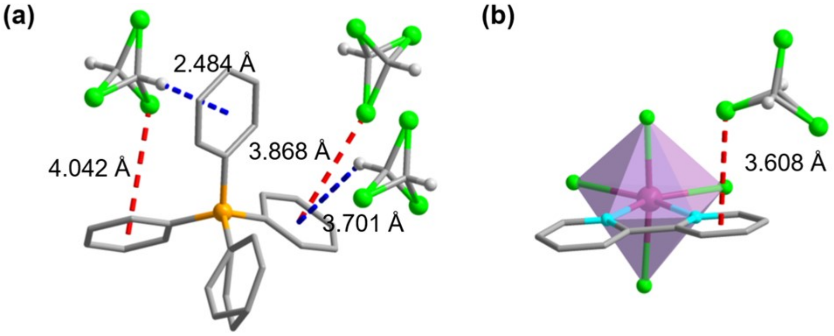

Fig S16. The intermolecular weak interactions between TCM molecules and the cations (a) or anions (b) in **2**. The C-H···π and Cl···π interactions are represented by blue and red dashed lines, respectively.

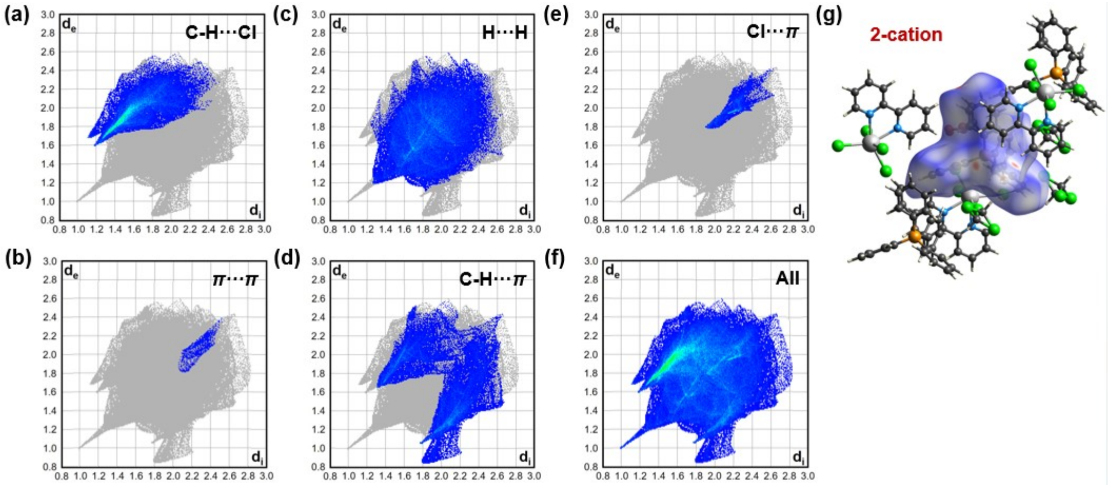

Fig S17. Two-dimensional fingerprint plot analysis: (a) C-H···Cl interactions, (b) π···π interactions, (c) H···H interactions, (d) C-H···π interactions, (e) Cl···π interactions, and (f) all interactions. (g) Hirshfeld surface mapped over d_{norm} of $[PPh_4]^+$ cation in **2**.

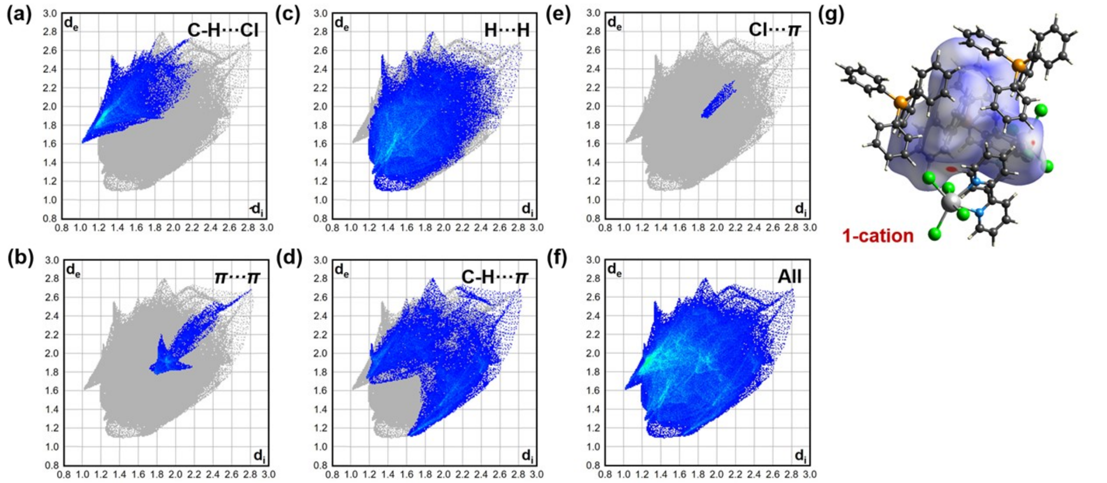

Fig S18. Two-dimensional fingerprint plot analysis: (a) C-H···Cl interactions, (b) π···π interactions, (c) H···H interactions, (d) C-H···π interactions, (e) Cl···π interactions, and (f) all interactions. (g) Hirshfeld surface mapped over d_{norm} of $[PPh_4]^+$ cation in **1**.

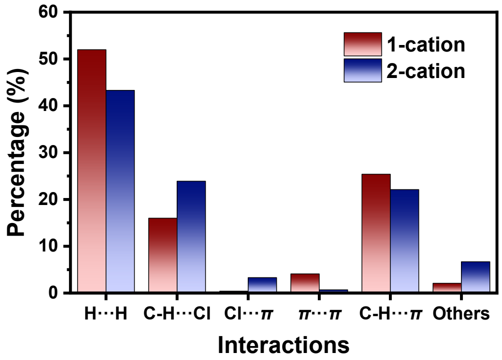

Fig S19. The intermolecular interactions of cations in **1** and **2** contribute to the Hirshfeld surface.

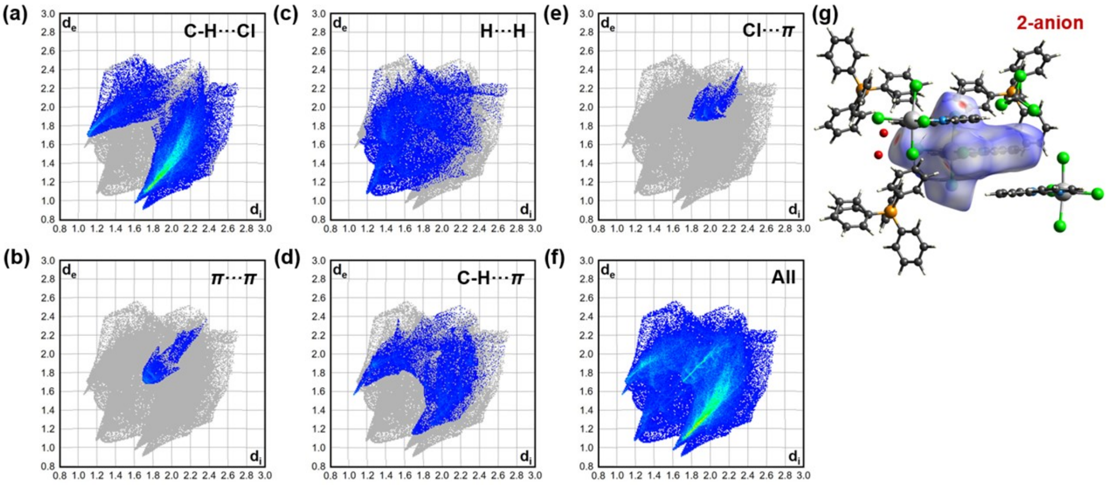

Fig S20. Two-dimensional fingerprint plot analysis: (a) C-H···Cl interactions, (b) π···π interactions, (c) H···H interactions, (d) C-H···π interactions, (e) Cl···π interactions, and (f) all interactions. (g) Hirshfeld surface mapped over d_{norm} of $[Bi(2,2'\text{-bpy})Cl_4]^-$ anion in **2**.

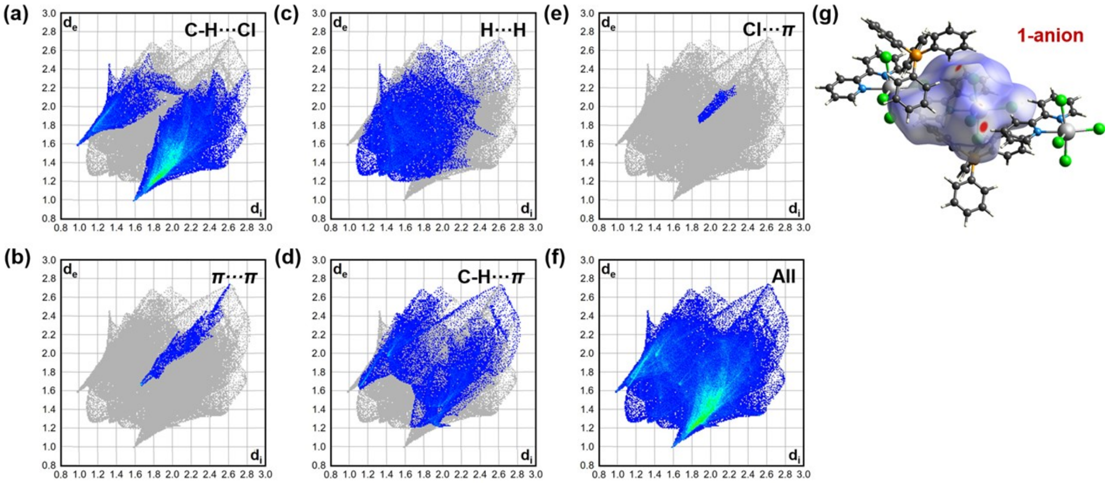

Fig S21. Two-dimensional fingerprint plot analysis: (a) C-H···Cl interactions, (b) π···π interactions, (c) H···H interactions, (d) C-H···π interactions, (e) Cl···π interactions, and (f) all interactions. (g) Hirshfeld surface mapped over d_{norm} of $[Bi(2,2'\text{-bpy})Cl_4]^-$ anion in **1**.

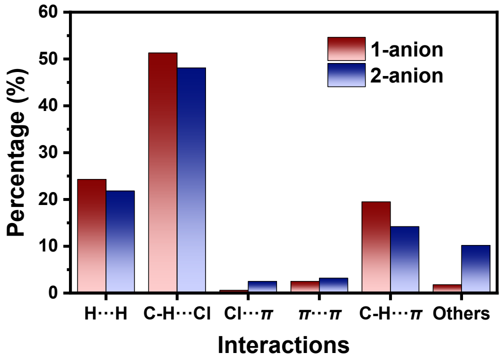

Fig S22. The intermolecular interactions of anions in **1** and **2** contribute to the Hirshfeld surface.

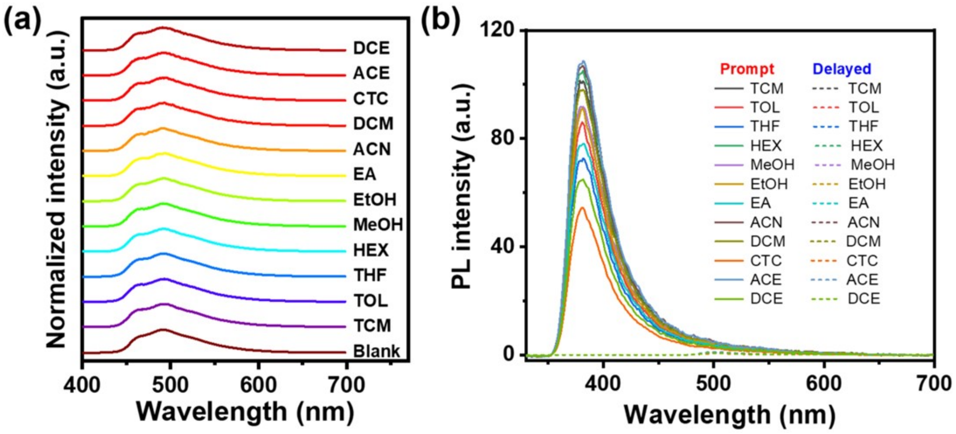

Fig S23. (a) Normalized delayed spectra of $[PPh_4]Cl$ after fumigation with various VOCs vapor (120 ppm) for 30 min. (b) Prompt (solid line) and delayed (dotted line) spectra of $[PPh_4]Cl$ in different solvents (1.0×10^{-4} M).

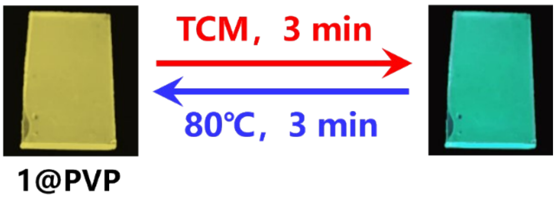

Fig S24. Photographs of **1**@PVP film fumigated with TCM vapor (120 ppm) for 3 min, and then heated at 80°C for 3 min under a 365 nm UV lamp.

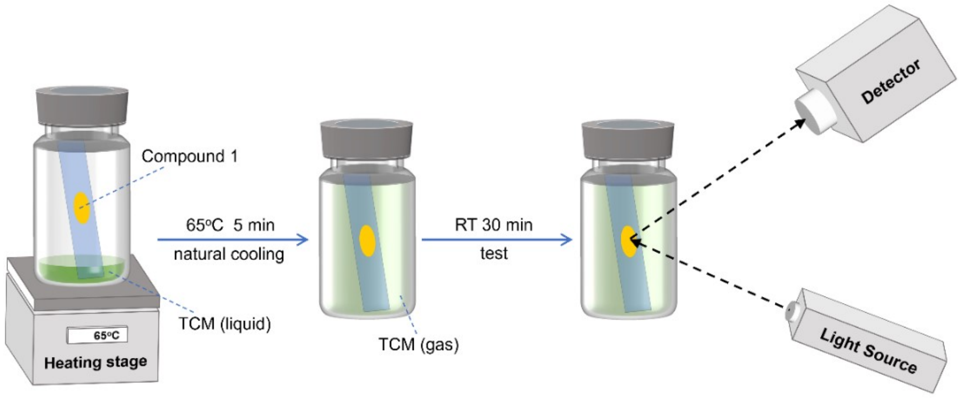

Fig. S25. Schematic diagram of a setup for TCM vapor sensing.

Table S1. TD-DFT calculated singlet and triplet energy levels of **1**.

Excited State	Energy/eV	λ/nm	f	Transition configuration/%
S_1	2.477	500.6	0.0182	HOMO-1→LUMO (46.9) HOMO→LUMO+1 (46.4)
S_2	2.655	467.0	0.0036	HOMO-1→LUMO+1 (34.1) HOMO-1→LUMO (27.5)
S_3	2.796	443.5	0.0109	HOMO-3→LUMO+2 (29.5) HOMO-6→LUMO+2 (26.3) HOMO-4→LUMO+3 (23.3)
S_4	2.937	422.2	0.0063	HOMO-7→LUMO+5 (37.1) HOMO-8→LUMO+2 (35.7) HOMO-4→LUMO+2 (18.2)
S_5	3.015	411.3	0.0147	HOMO-1→LUMO+5 (40.7) HOMO-8→LUMO+2 (22.2) HOMO→LUMO+10 (10.1)
T_1	2.016	615.1	-	HOMO→LUMO (62.7) HOMO-1→LUMO (19.1)
T_2	2.320	534.5	-	HOMO-1→LUMO+1 (58.0) HOMO→LUMO+1 (22.8)
T_3	2.729	454.4	-	HOMO-3→LUMO+2 (53.6) HOMO-4→LUMO+2 (15.1) HOMO-2→LUMO+3 (8.9)
T_4	2.848	435.4	-	HOMO-1→LUMO+4 (28.5) HOMO-6→LUMO+2 (19.3) HOMO-2→LUMO+3 (2.4)
T_5	2.971	417.4	-	HOMO→LUMO+7 (39.4) HOMO-2→LUMO+4 (21.7) HOMO-6→LUMO+2 (3.0)

Table S2. TD-DFT calculated singlet and triplet energy levels of **2**.

Excited State	Energy/eV	λ/nm	f	Transition configuration/%
S_1	2.302	538.7	0.0108	HOMO→LUMO+2 (48.5) HOMO-1→LUMO+3 (47.0) HOMO→LUMO (10.2)
S_2	2.425	511.3	0.0019	HOMO-1→LUMO+1 (58.0) HOMO→LUMO+1 (22.8) HOMO-2→LUMO (6.23)
S_3	2.771	447.5	0.0035	HOMO-3→LUMO+2 (53.6) HOMO-4→LUMO+2 (15.1) HOMO-2→LUMO+3 (8.9) HOMO-1→LUMO+4 (2.3)

S_4	2.859	433.7	0.0080	HOMO-5→LUMO+4 (68.5) HOMO-6→LUMO+2 (19.3) HOMO-2→LUMO+3 (2.4)
S_5	2.980	416.1	0.0002	HOMO-3→LUMO+7 (59.4) HOMO-2→LUMO+4 (21.7)
T_1	2.096	591.6	-	HOMO→LUMO+2 (52.9) HOMO→LUMO+3(20.8) HOMO-1→LUMO+2 (9.1)
T_2	2.179	569.1	-	HOMO-1→LUMO+3 (47.0) HOMO-2→LUMO+1 (23.1)
T_3	2.507	494.6	-	HOMO-1→LUMO (46.6) HOMO→LUMO+1 (33.1)
T_4	2.667	464.9	-	HOMO-1→LUMO+4 (25.0) HOMO-3→LUMO+5 (17.6) HOMO→LUMO+7 (7.2) HOMO-5→LUMO+1 (4.0)
T_5	2.793	444.0	-	HOMO-3→LUMO+7 (33.0) HOMO→LUMO+5 (9.8) HOMO-6→LUMO+1 (7.6)

Table S3. The S_n/T_n spin-orbit coupling (SOC) constants (ξ) of **1**.

S_n/T_n	ξ / cm^{-1}	S_n/T_n	ξ / cm^{-1}
S_0-T_1	1.518	S_1-T_1	1.863
S_0-T_2	29.437	S_1-T_2	9.672
S_0-T_3	5.296	S_1-T_3	0.088
S_0-T_4	5.073	S_2-T_1	1.323
S_0-T_5	1.082	S_2-T_2	2.385
		S_2-T_3	0.137

Table S4. The S_n/T_n spin-orbit coupling (SOC) constants (ξ) of **2**.

S_n/T_n	ξ / cm^{-1}	S_n/T_n	ξ / cm^{-1}
S_0-T_1	2.703	S_1-T_1	1.661
S_0-T_2	2.972	S_1-T_2	0.254
S_0-T_3	51.718	S_2-T_1	0.024
S_0-T_4	5.181	S_2-T_2	0.049
S_0-T_5	6.840	S_3-T_1	0.097
		S_3-T_2	1.180
		S_3-T_3	16.947

Table S5. Crystallographic data for compounds **1** and **2**.

	1	**2**
Empirical formula	$C_{34}H_{28}Cl_4N_2PBi$	$C_{35}H_{30}Cl_7N_2O_{0.5}PBi$
Formula weight	846.33	974.71
Temperature (K)	296(2)	120(2)
Crystal system	Triclinic	Triclinic
space group	P-1	P-1
a (Å)	9.3023(9)	8.948(3)
b (Å)	12.9358(14)	13.456(5)
c (Å)	14.6401(17)	17.067(6)
α (°)	104.068(4)	71.085(11)
β (°)	102.057(4)	76.978(12)
γ (°)	90.055(4)	83.504(12)
Volume (A^3)	1668.7(3)	1892.2(12)
Z, Calculated density (Mg/m^3)	2, 1.684	2, 1.711
Absorption coefficient (mm^{-1})	5.678	5.225
F(000)	824	950
Theta range for data collection (deg.)	2.697 to 27.591	2.344 to 25.000
Limiting indices	-12<=h<=12, -16<=k<=16, -19<=l<=18	-10<=h<=10, -15<=k<=15, -20<=l<=20
Reflections collected / unique	47098 / 7686 [R(int) = 0.0599]	72720 / 6648 [R(int) = 0.0978]
Completeness to theta = 25.242	99.8%	97.0 %
Absorption correction	Multi scan	Multi scan
Max. and min. transmission	0.7456 and 0.2174	0.7455 and 0.5332
Refinement method	Full-matrix least-squares on F^2	Full-matrix least-squares on F^2
Goodness-of-fit on F^2	1.083	1.049
Final *R indices [I>2sigma(I)]	*R_1 = 0.0318, **wR_2 = 0.0804	*R_1 = 0.0354, **wR_2 = 0.0870
*R indices (all data)	*R_1 = 0.0363, **wR_2 = 0.0830	*R_1 = 0.0448, **wR_2 = 0.0908
Largest diff. peak and hole ($e.A^{-3}$)	1.563 and -2.228	1.243 and -1.285

*R= $\sum(||F_o|-|F_c||) / \sum |F_o|$, **wR = $\{\sum w [(F^2_o - F^2_c)] / \sum w [(F^2_o)^2]\}^{0.5}$,

w = $[\sigma^2(F^2_o) + (aP)^2+bP]^{-1}$, where P = $(F^2_o + 2 F^2_c)/3$. Compound **1**: a = 0.0468, b = 1.2934; Compound **2**: a = 0.0495, b = 3.4523.

Table S6. Selected bond lengths (Å) and angles (°) for compounds **1** and **2**.

1		**2**	
Bi(1)-N(1)	2.442(3)	Bi(1)-N(1)	2.453(5)
Bi(1)-N(2)	2.488(4)	Bi(1)-N(2)	2.470(5)
Bi(1)-Cl(3)	2.6579(11)	Bi(1)-Cl(4)	2.6800(15)
Bi(1)-Cl(4)	2.6752(15)	Bi(1)-Cl(2)	2.7207(17)
Bi(1)-Cl(1)	2.6780(12)	Bi(1)-Cl(1)	2.7256(15)
Bi(1)-Cl(2)	2.7076(13)	Bi(1)-Cl(3)	2.7376(16)
P(1)-C(29)	1.789(5)	P(1)-C(17)	1.792(6)
P(1)-C(11)	1.791(4)	P(1)-C(23)	1.797(6)
P(1)-C(17)	1.794(4)	P(1)-C(29)	1.803(6)
P(1)-C(23)	1.800(4)	P(1)-C(11)	1.805(6)
N(1)-C(1)	1.328(6)	N(1)-C(1)	1.338(8)
N(1)-C(5)	1.349(5)	N(1)-C(5)	1.366(7)
N(2)-C(10)	1.339(6)	N(2)-C(10)	1.345(7)
N(2)-C(6)	1.347(5)	N(2)-C(6)	1.356(7)
N(1)-Bi(1)-N(2)	65.95(12)	N(1)-Bi(1)-N(2)	66.85(16)
N(1)-Bi(1)-Cl(3)	81.40(9)	N(1)-Bi(1)-Cl(4)	81.81(12)
N(2)-Bi(1)-Cl(3)	89.01(8)	N(2)-Bi(1)-Cl(4)	87.38(11)
N(1)-Bi(1)-Cl(4)	89.71(9)	N(1)-Bi(1)-Cl(2)	89.66(12)
N(2)-Bi(1)-Cl(4)	154.34(9)	N(2)-Bi(1)-Cl(2)	156.31(11)
Cl(3)-Bi(1)-Cl(4)	95.54(5)	Cl(4)-Bi(1)-Cl(2)	92.33(6)
N(1)-Bi(1)-Cl(1)	84.73(9)	N(1)-Bi(1)-Cl(1)	83.08(12)
N(2)-Bi(1)-Cl(1)	77.62(9)	N(2)-Bi(1)-Cl(1)	83.50(11)
Cl(3)-Bi(1)-Cl(1)	163.78(5)	Cl(4)-Bi(1)-Cl(1)	164.49(4)
Cl(4)-Bi(1)-Cl(1)	92.77(6)	Cl(2)-Bi(1)-Cl(1)	91.04(6)
N(1)-Bi(1)-Cl(2)	156.67(10)	N(1)-Bi(1)-Cl(3)	154.74(12)
N(2)-Bi(1)-Cl(2)	91.45(9)	N(2)-Bi(1)-Cl(3)	88.04(11)
Cl(3)-Bi(1)-Cl(2)	92.98(4)	Cl(4)-Bi(1)-Cl(3)	94.89(5)
Cl(4)-Bi(1)-Cl(2)	113.44(5)	Cl(2)-Bi(1)-Cl(3)	115.55(5)
Cl(1)-Bi(1)-Cl(2)	96.46(5)	Cl(1)-Bi(1)-Cl(3)	97.29(5)
C(29)-P(1)-C(11)	109.1(2)	C(17)-P(1)-C(23)	110.0(3)
C(29)-P(1)-C(17)	108.4(2)	C(17)-P(1)-C(29)	108.6(3)
C(11)-P(1)-C(17)	110.46(19)	C(23)-P(1)-C(29)	111.3(3)
C(29)-P(1)-C(23)	108.7(2)	C(17)-P(1)-C(11)	110.7(3)
C(11)-P(1)-C(23)	111.2(2)	C(23)-P(1)-C(11)	107.9(3)
C(17)-P(1)-C(23)	108.8(2)	C(29)-P(1)-C(11)	108.2(3)
C(1)-N(1)-C(5)	120.0(4)	C(1)-N(1)-C(5)	119.2(5)
C(1)-N(1)-Bi(1)	120.0(3)	C(1)-N(1)-Bi(1)	121.0(4)
C(5)-N(1)-Bi(1)	120.0(3)	C(5)-N(1)-Bi(1)	119.6(4)
C(10)-N(2)-C(6)	119.7(4)	C(10)-N(2)-C(6)	119.1(5)
C(10)-N(2)-Bi(1)	120.4(3)	C(10)-N(2)-Bi(1)	121.3(4)
C(6)-N(2)-Bi(1)	117.6(3)	C(6)-N(2)-Bi(1)	119.5(4)

III. Supplementary References.

1 G. M. Sheldrick, Acta Crystallogr. C, 2015, **71**, 3–8.

2 M. J. Frisch, G. W. Trucks, H. B. Schlegel, G. E. Scuseria, M. A. Robb, J. R. Cheeseman, G. Scalmani, V. Barone, B. Mennucci, G. A. Petersson, H. Nakatsuji, M. Caricato, X. Li, H. P. Hratchian, A. F. Izmaylov, J. Bloino, G. Zheng, J. L. Sonnenberg, M. Hada, M. Ehara, K. Toyota, R. Fukuda, J. Hasegawa, M. Ishida, T. Nakajima, Y. Honda, O. Kitao, H. Nakai, T. Vreven, J. A. Montgomery, J. E. Peralta, F. Ogliaro, M. Bearpark, J. J. Heyd, E. Brothers, K. N. Kudin, V. N. Staroverov, R. Kobayashi, J. Normand, K. Raghavachari, A. Rendell, J. C. Burant, S. S. Iyengar, J. Tomasi, M. Cossi, N. Rega, J. M. Millam, M. Klene, J. E. Knox, J. B. Cross, V. Bakken, C. Adamo, J. Jaramillo, R. Gomperts, R. E. Stratmann, O. Yazyev, A. J. Austin, R. Cammi, C. Pomelli, J. W. Ochterski, R. L. Martin, K. Morokuma, V. G. Zakrzewski, G. A. Voth, P. Salvador, J. J. Dannenberg, S. Dapprich, A. D. Daniels, O. Farkas, J. B. Foresman, J. V. Ortiz, J. Cioslowski and D. J. Fox, Gaussian 16, Revision A.03, Gaussian, Inc., Wallingford, CT, 2016.

3 J.-D. Chai, M. Head-Gordon, Phys. Chem. Chem. Phys., 2008, **10**, 6615–6620.

4 T. Lu and F. Chen, J. Comput. Chem., 2012, **33**, 580–592.

5 Z. Liu, T. Lu and Q. Chen, Carbon, 2020, **165**, 461–467.

6 F. Neese, Wires. Comput. Mol. Sci., 2012, **2**, 73–78; F. Neese, Wires Comput. Mol. Sci., 2018, **8**, e1327.